Supporting Information

for

High-pressure behavior of 3.65 Å phase: Insights from Raman spectroscopy

Abhisek Basu[1,*], Mainak Mookherjee[1], Christelle Bucag[1], Sergey Tkachev[2], Bernd Wunder[3]

[1]Earth Materials Laboratory, Earth, Ocean and Atmospheric Science, Florida State University, Tallahassee, Florida 32306, USA

[2]Center for Advanced Radiation Sources, University of Chicago, Chicago, Illinois 60637, USA

[3]Deutsches GeoForschungsZentrum GFZ, Section 3.6, Telegrafenberg, 14473 Potsdam, Germany

*abasu@fsu.edu

Content:

Supporting Figure SF1: Raman spectra of the hydroxyl stretching region between 3000- 3500 cm^{-1} of 3.65 Å phase inside diamond anvil cell (DAC), collected at ambient conditions. The stack shows incremental steps in which laser power was increased from 10%, 25 %, 50 %, and 100 % of 300 mW at the source. The hydroxyl stretching modes remain unaffected as a function of incident laser power.

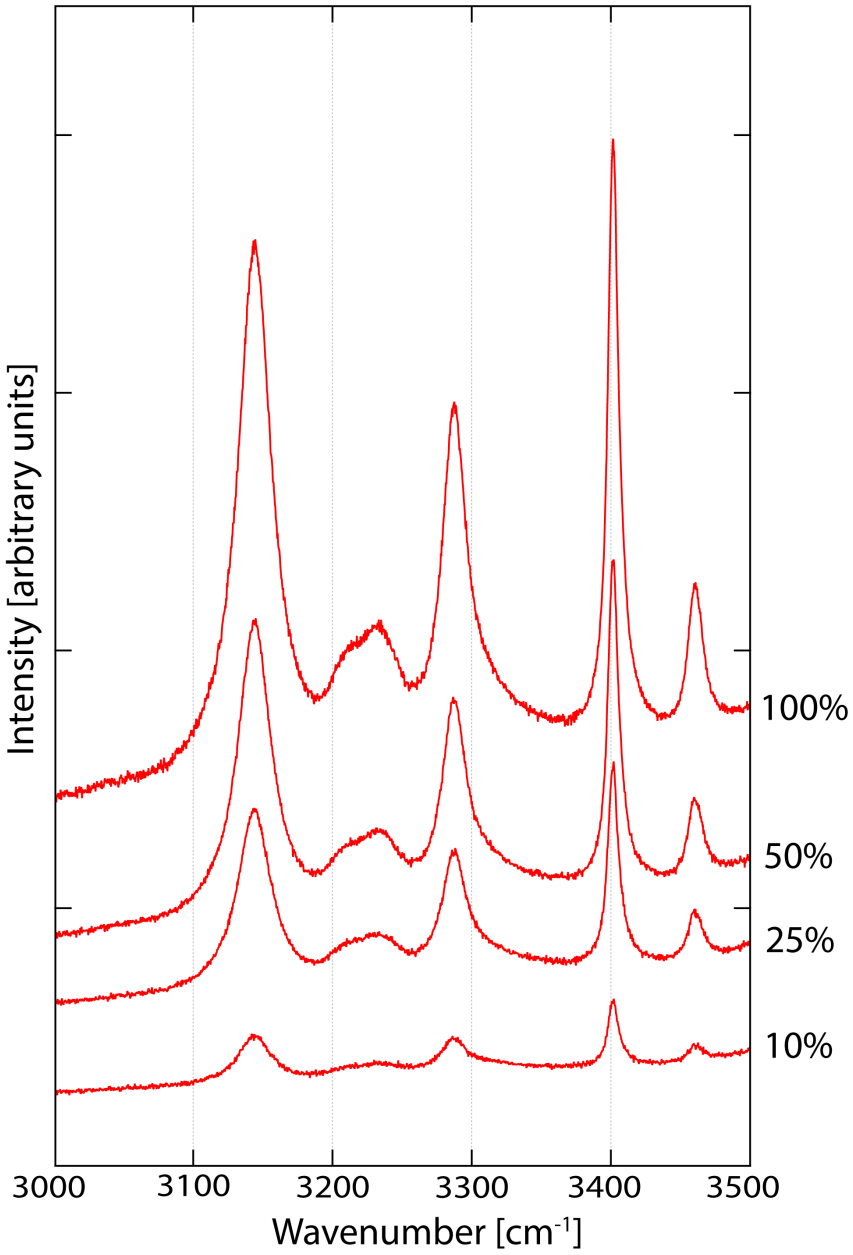

Supporting Figure SF2: Low wavenumber Raman spectra of the 3.65 Å phase collected at ambient conditions. The deconvolution reveals 22 modes in the region from 150 cm^{-1} to 1300 cm^{-1}.

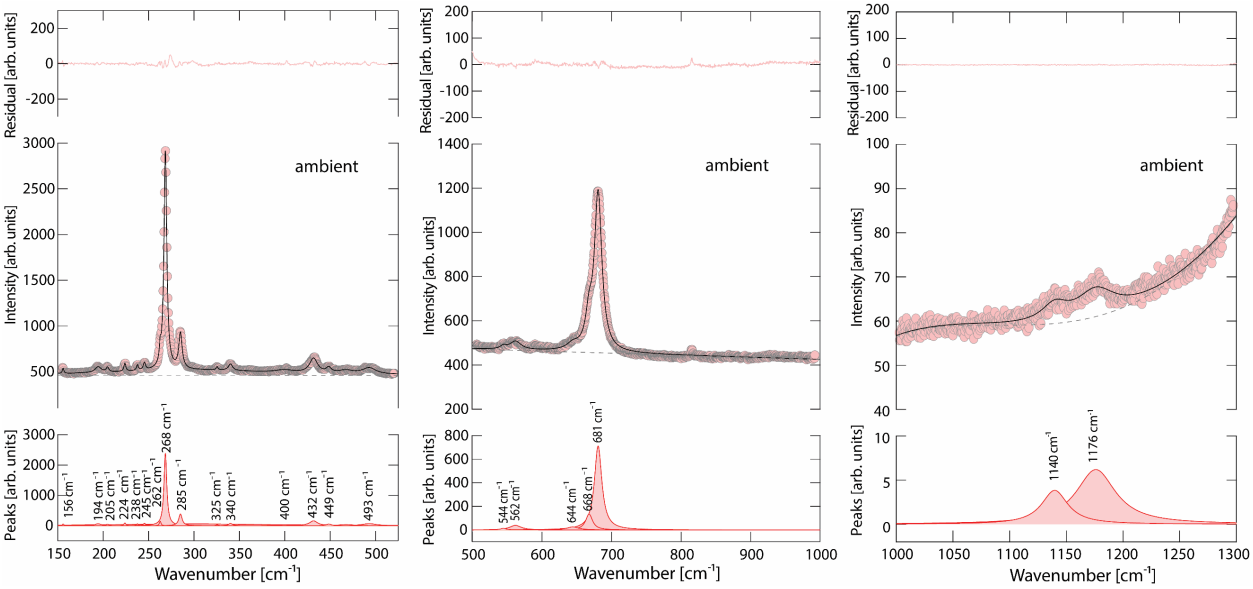

Supporting Figure SF3: Low wavenumber Raman spectra of the 3.65 Å phase collected at 7.9 GPa.

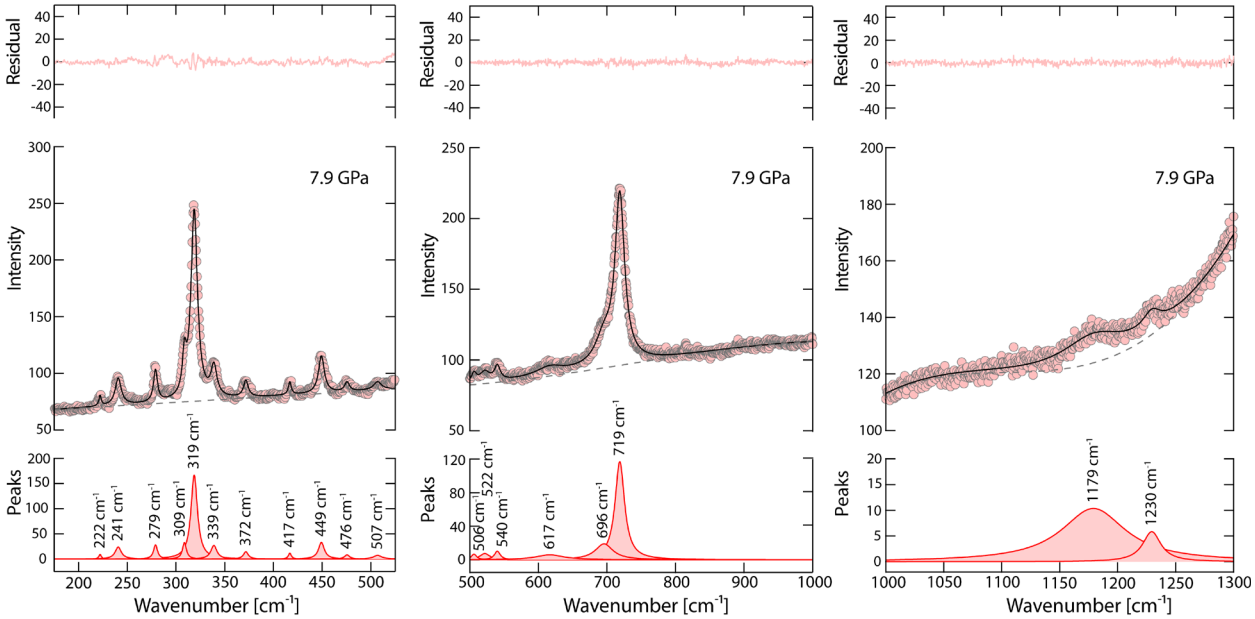

Supporting Figure SF4: Deconvoluted Raman spectra of the hydroxyl stretching region for the 3.65 Å phase at **(a)** ambient conditions; **(b)** 4.3 GPa; and **(c)** 16 GPa. The Raman spectra (solid pink circles) are fitted to a Lorentzian curve (solid black line). The baseline is shown in a dashed gray line and individual Lorentzian peaks are shown at the bottom.

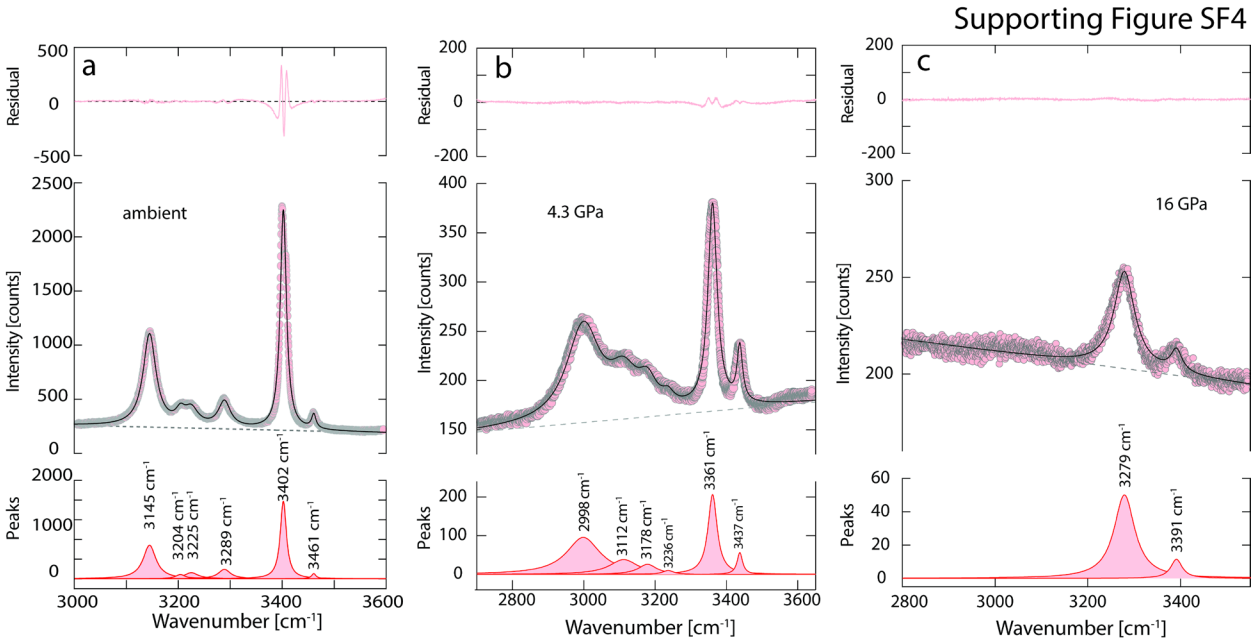

Supporting Figure SF5: Plot of the phase stability of mineral phases [Coe: coesite; St: stishovite; LPCen: low-pressure clinoenstatite; OEn: orthoenstatite; HPCen: high-pressure clinoenstatite]. The solid dark gray line indicates the water-ice VII phase boundary. The dotted blue line indicates Tonga slab geotherm (Peacock 1990). The dashed lines indicate the lowest temperature predicted in the Tonga slab (Wei et al. 2017). (MTZ: mantle transition zone).

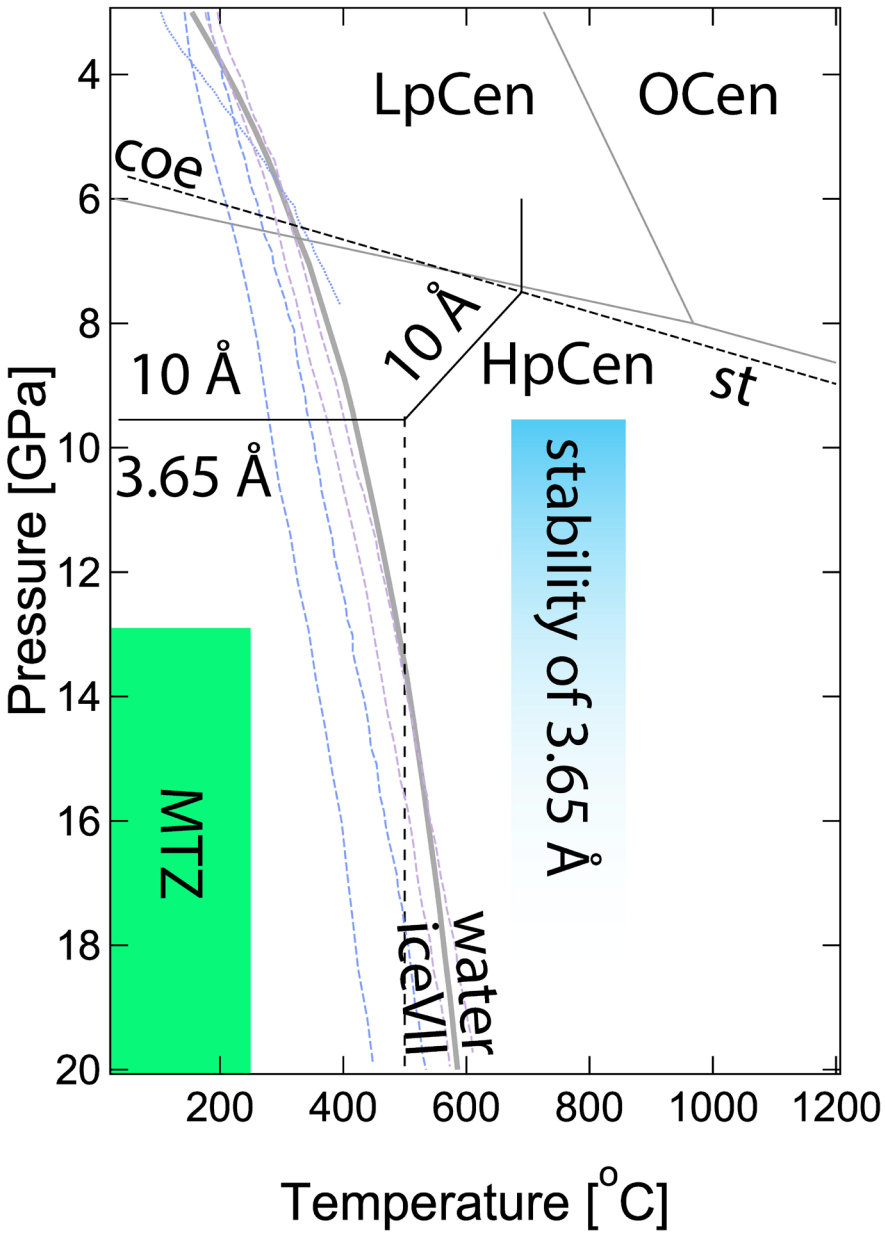

Supporting Figure SF6: Comparison of spectral peak widths of hydroxyl stretching modes (ν_1^{OH}) and (ν_2^{OH}) as a function of pressure from five compression runs using a neon and alcohol mixture as the pressure medium. The dashed gray line is the polynomial fit to the mode widths. A marked increase is observed in the widths from ~5 GPa onwards. Error bars represent 1σ uncertainties.

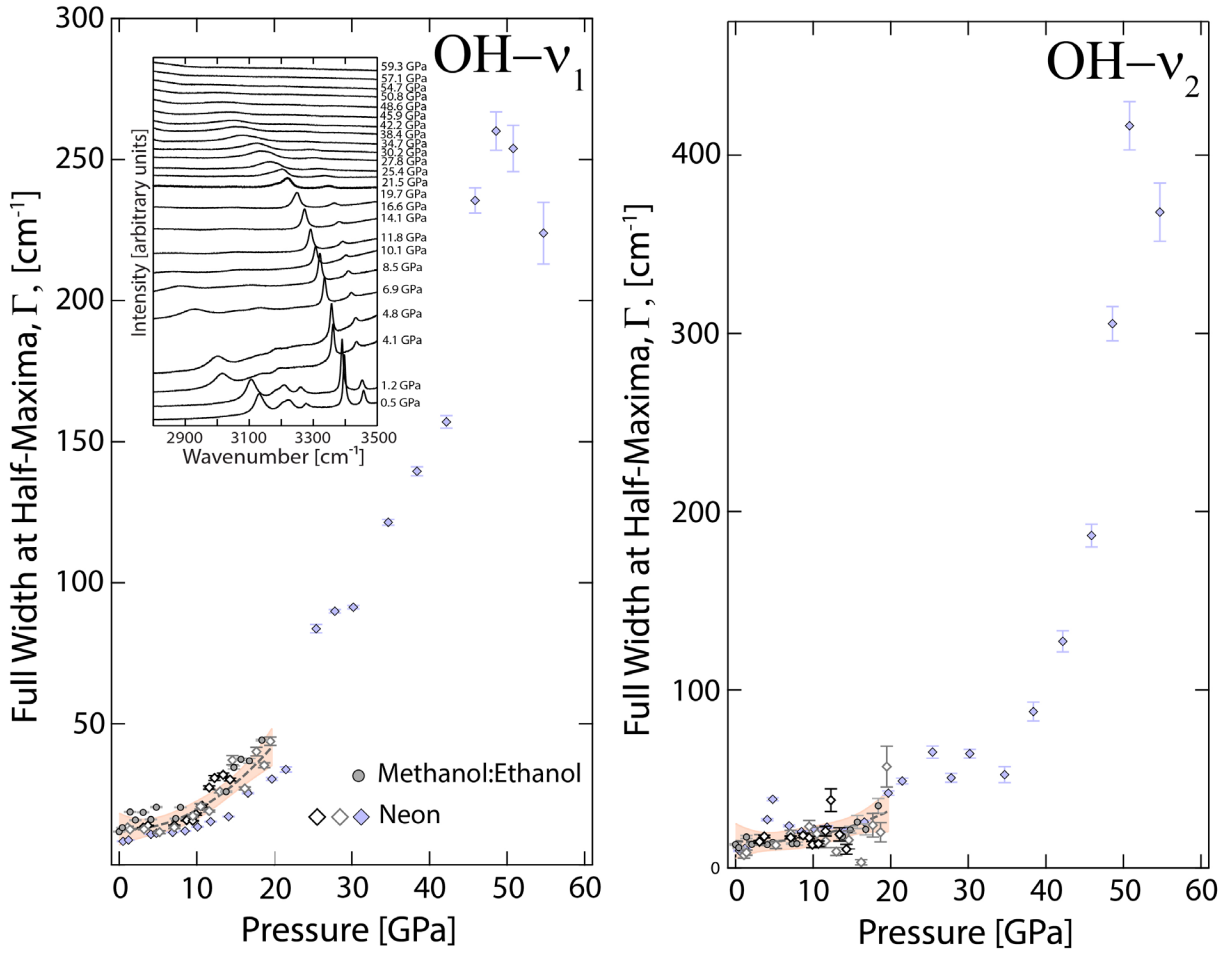

Supporting Figure SF7: Plot of the OH-stretching frequencies with the hydrogen bond length ($R_{OH...O}$) of the 3.65 Å phase (violet solid circles). The regression curves are polynomial fits to OH-stretching modes and the corresponding hydrogen bond length of different minerals (red: Libowitzky 1999; gray: Goryainov 2012).

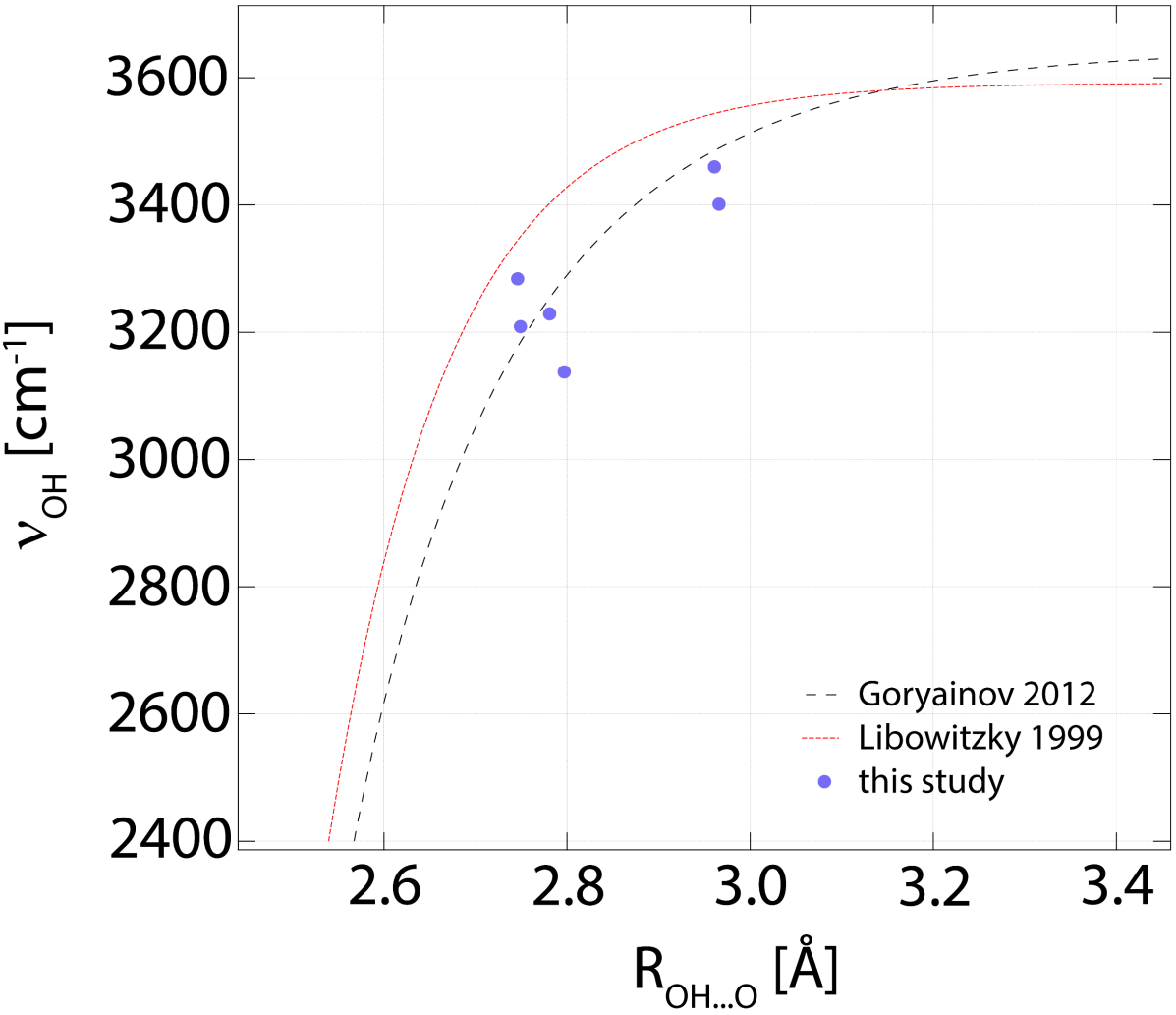

Supporting Table ST1: Details of experimental conditions explored in this study.

Expt. #	*Diamond*	*Culet* [μm]	*Pressure Media*	P_{min} [GPa]	P_{max} [GPa]
1	Low fluorescence Type Ia	300	Methanol:Ethanol	0.0001	20.0
2				0.0001	18.4
3			Neon	3.1	14.3
4				1.1	19.4
5				0.5	59.3

Supporting Table ST2: Deconvoluted Raman mode frequencies of the hydroxyl stretching vibrations at ambient conditions. The responsible O-H stretching motion for individual modes is taken from Wunder (2012). The values in parenthesis are mode assignments from Borodina (2020).

Mode frequency [cm^{-1}]						
Wunder (2012)	*Borodina (2020)*	*This study*	*Bond*	*Length (Å)*	*Bond*	*Length (Å)*
3455 3382	3404	3402	O1-H1	1.024	H1…O1	1.937
3462 3389	3463	3461	O2-H2	0.928	H2…O2	2.045
3175 3099	3147	3145	O3-H4	1.059	H4…O6	1.698
3205 3180		3204	O4-H3	0.969	H3…O5	1.821
3300 3278	3291	3289	O5-H5	0.921	H5…O3	1.841
3231 3096	3225	3225	O6-H6	0.939	H6…O4	1.857

Supporting Table ST3: Pressure-dependence of the Raman modes of the 3.65 Å phase and expansion coefficients up to 60 GPa.

Modes	ν_{i0}	$\sigma\nu_{i0}$	b_i	σb_i	c_i	σc_i
1	204.7	1.1	1.99	0.12	-0.02	0.00
2	203.9	0.5	5.48	0.15	-0.06	0.01
3	227.7	1.1	3.26	0.14	-0.02	0.00
4	238.5	0.6	4.68	0.28	-0.20	0.03
5	245.8	0.3	4.11	0.20	-0.07	0.03
6	264.8	1.1	1.98	0.32	-0.02	0.02
7	250.2	9.5	4.76	0.92	-0.07	0.02
8	270.1	1.1	5.65	0.27	-0.66	0.01
9	288.6	1.0	4.57	0.12	-0.04	0.00
10	303.0	1.3	4.14	0.14	-0.02	0.00
11	326.4	0.4	4.23	0.08	-0.04	0.00
12	341.8	0.6	4.26	0.12	-0.05	0.00
13	402.2	0.5	2.00	0.05	-0.01	0.00
14	431.3	1.1	2.46	0.20	0.00	0.01
15	442.6	3.0	3.55	0.40	0.01	0.01
16	471.8	1.1	6.53	0.17	-0.06	0.01
17	494.3	1.2	6.60	0.41	-0.07	0.02
18	568.2	1.9	6.67	0.44	-0.04	0.02
19	665.9	1.9	3.40	0.25	-0.02	0.00
20	682.9	1.4	4.60	0.14	-0.02	0.00
21	647.5	14.6	7.10	1.35	-0.08	0.03
22	1139.7	3.0	5.36	0.76	-0.08	0.04
23	1182.7	2.6	6.58	0.76	-0.04	0.04
24 (OH -ν_3)	3146.8	0.0	-34.54	0.05	0.46	0.01
25 (OH -ν_4)	3206.8	0.2	-20.08	0.13	-0.43	0.02
26 (OH -ν_6)	3228.5	2.3	-10.63	1.20	-0.13	0.09
27 (OH -ν_5)	3286.4	3.3	-18.52	2.80	1.49	0.42
28 (OH -ν_1)	3405.5	2.5	-9.71	0.30	-0.03	0.01
29 (OH -ν_2)	3460.1	1.5	-5.26	0.19	0.00	0.00

Note: Subscript "*i*" refers to the vibrational modes. The pressure dependence of the modes is described by an expansion of the form $\nu_i = \nu_{i0} + b_i P + c_i P^2$ where b_i refers to the first derivative $\frac{\partial \nu_i}{\partial P}$ and c_i refers to the second derivative $\frac{\partial^2 \nu_i}{\partial P^2}$. The ν_{i0} is the mode frequency at P_0 of 1×10^{-4} GPa. Errors represent 1σ uncertainties.

Supporting Table ST4: Pressure dependency of Raman frequencies and derived values of $\frac{K_0}{K_0'}$ for the 3.65 Å phase.

Modes	ν_{i0}	$\sigma\nu_{i0}$	b_i	σb_i	c_i	σc_i	$1/(b_i/a_i - 2c_i/b_i)$	*Error*
1	198.4	1.0	3.80	0.22	-0.10	0.01	13.6	1.6
2	203.9	0.5	5.48	0.15	-0.06	0.01	20.5	2.8
3	226.0	1.1	3.89	0.33	-0.05	0.02	23.0	8.5
4	238.5	0.6	4.68	0.28	-0.20	0.03	9.6	1.4
5	245.8	0.3	4.11	0.20	-0.07	0.03	19.5	7.1
6	264.8	1.1	1.98	0.32	-0.02	0.02	36.3	36.0
8	270.3	1.1	5.53	0.28	-0.06	0.01	24.2	6.2
9	288.2	1.0	4.49	0.27	-0.02	0.01	38.0	22.3
10	298.9	1.4	5.60	0.34	-0.09	0.02	19.2	3.7
11	326.0	0.3	4.52	0.10	-0.06	0.01	26.1	2.8
12	340.8	0.5	4.75	0.15	-0.08	0.01	20.9	2.2
13	402.3	0.4	2.09	0.10	-0.01	0.01	58.6	24.5
14	432.0	1.2	2.14	0.33	0.02	0.02	-91.3	-92.4
15	446.2	3.3	1.93	0.90	0.09	0.05	-11.0	-7.8
16	470.8	1.1	6.99	0.28	-0.09	0.02	24.7	4.3
17	494.3	1.2	6.60	0.41	-0.07	0.02	28.1	9.5
18	567.7	2.0	6.88	0.51	-0.06	0.03	34.9	17.6
19	664.2	2.8	4.07	0.83	-0.06	0.04	29.2	22.9
20	681.4	0.8	5.09	0.21	-0.04	0.01	40.2	10.2
22	1140.3	3.1	5.08	0.84	-0.06	0.04	33.9	24.1
23	1182.7	2.6	6.58	0.76	-0.04	0.04	54.3	54.1
24-OH-3	3146.8	0.0	-34.54	0.05	0.46	0.01	63.7	1.2
25-OH-4	3206.8	0.2	-20.08	0.13	-0.43	0.02	-20.3	-0.9
26-OH-6	3230.3	0.2	-9.51	0.10	-0.12	0.01	-34.7	-1.8
27-OH-5	3291.0	0.0	-28.33	0.12	3.45	0.03	4.3	0.0
28-OH-1	3403.2	0.0	-9.37	0.00	0.06	0.00	98.7	0.5
29-OH-2	3458.8	2.0	-4.97	0.50	-0.01	0.00	-201.6	-24.3